WATER RESOURCES RESEARCH, VOL. 24, NO. 1, PAGES 115–126, JANUARY 1988

Analytical Models of Slug Tests

K. KARASAKI, J. C. S. LONG, AND P. A. WITHERSPOON

Earth Sciences Division, Lawrence Berkeley Laboratory, University of California, Berkeley

In the present paper, attempts are made to develop solutions to various models of slug tests that may be applicable in analyzing the results of such tests where existing solutions are inadequate. Various geometries that may be encountered in heterogeneous systems such as fractured rocks are considered. Solutions are presented for linear flow, radial flow with boundaries, two layer, and concentric composite models with different flow geometries between the inner and outer region. Solutions are obtained in Laplace space and inverted back to real space numerically. Type curves are presented for each solution. Analyses of the type curves and derivative response curves reveal that many curves have unique shapes only for certain combination of the flow parameters and the distance. Other sets of type curves are similar in shape, although log-log plots and derivative plots may emphasize some features that may not be apparent in semilog plots. These results show that slug tests suffer problems of nonuniqueness to a greater extent than other well tests.

INTRODUCTION

Slug tests were originally developed for estimating flow parameters of shallow aquifers, which are often well-approximated as homogeneous porous media. They have also been widely used to estimate the flow parameters of heterogeneous systems such as fractured rocks. The attractiveness of slug tests is that they are inexpensive and easy to perform and require a relatively short time to complete. However, available analysis methods for slug tests are limited to a few ideal cases. In the present paper, attempts are made to develop solutions to various models of slug tests that may be applicable in analyzing the results of such tests where existing solutions are inadequate. Throughout the paper, it is assumed that the inertial effects in the well is negligible.

Cooper et al. [1967] presented a solution for the change in water level for a finite radius well subjected to a slug test in a homogeneous medium. They showed that the instantaneous line-source solution proposed by *Ferris and Knowles* [1954] is valid only for very late time. Cooper et al. obtained the solution from the analogous heat transfer problem by *Carslaw and Jaeger* [1946]. The transient water level $h_s(r_D, t_s)$ at any point in an aquifer normalized to the initial level in the well is

$$h_s(r_D, t_s) = \frac{2}{\pi} \int_0^\infty e^{-t_s\mu^2/\omega} \frac{\{J_0(\mu r_D)\Psi(\mu) - Y_0(\mu r_D)\Phi(\mu)\}}{\Phi^2(\mu) + \Psi^2(\mu)} \, d\mu \quad (1)$$

where

$$h_s = (h - h_i)/(h_0 - h_i) \quad (2)$$

$$t_s = 2\pi T t / C_w = t_D \omega \quad (3)$$

$$\omega = 2\pi r_w^2 S / C_w \quad (4)$$

$$r_D = r/r_w \quad (5)$$

$$\Phi(\mu) = \mu J_0(\mu) - \omega J_1(\mu) \quad (6)$$

$$\Psi(\mu) = \mu Y_0(\mu) - \omega Y_1(\mu) \quad (7)$$

and T is the transmissivity of the formation, S is the storativity of the formation, and C_w is the well bore storage. For an open hole slug test, $C_w = \pi r_a^2$, where r_a is the radius of the delivery pipe. It must be noted that in the present paper ω is used in place of α in Cooper et al.'s paper. The list of notations appears at end of the paper.

Specifically, for $r_D = 1$, where h_s equals the water level in the well, h_{w_s},

$$h_{w_s}(t) = \frac{4\omega}{\pi^2} \int_0^\infty e^{-t_s\mu^2/\omega} \frac{d\mu}{\mu[\Phi^2(\mu) + \Psi^2(\mu)]} \quad (8)$$

Cooper et al. evaluated (8) and presented type curves as shown in Figure 1. Figure 1 can be used to estimate the transmissivity and the storativity by curve matching.

Several workers have investigated the effects of skin on observed fluid levels on slug tests [*Ramey and Agarwal*, 1972; *Ramey et al.*, 1975; *Faust and Mercer*, 1984; *Moench and Hsieh*, 1985; *Sageev*, 1986]. *Wang et al.* [1977] studied cases where tight fractures intersect the well bore. *Barker and Black* [1983] presented a solution for slug tests in a double porosity medium. However, not many other different solutions have been developed for slug tests. In the present paper we extend the available solutions to various geometries that may be encountered in heterogeneous systems such as fractured rocks.

The Laplace transformation is the analytical tool best suited to problems where the boundary conditions involve a time derivative. Throughout this paper, the Laplace transformation is used to eliminate the time variable and solutions are obtained in Laplace space. Even though analytical inversions are possible following steps similar to those in *Karasaki et al.* [1988], the solutions will be in the form of infinite integrals of Bessel functions which converge extremely slowly. Thus in many cases, solutions must be evaluated numerically, which is much more time consuming. In the present paper therefore the numerical inversion scheme developed by *Stehfest* [1970] is used for most cases. Because the arithmetics followed in obtaining the solutions in Laplace space are similar in most cases, only two solution schemes are detailed in the appendix. The solution schemes for the rest can be found in the work by *Karasaki* [1986].

LINEAR FLOW MODEL

When a test interval intercepts a large, highly conductive fracture, the pressure drop along the fracture plane may be negligible compared to the formation, and the flow in the

Paper number 6W4761.
0043-1397/88/006W-4761$05.00

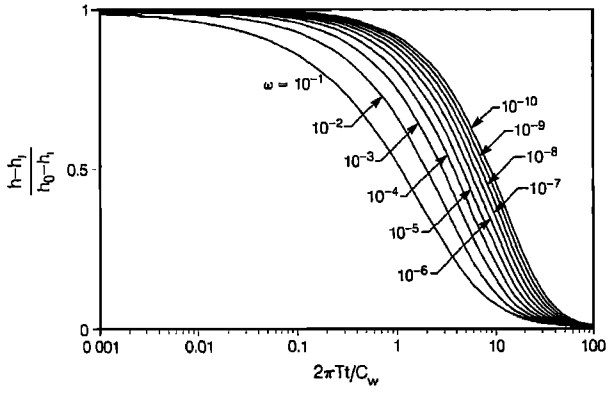

Fig. 1. Type curves for radial flow after *Cooper et al.* [1967].

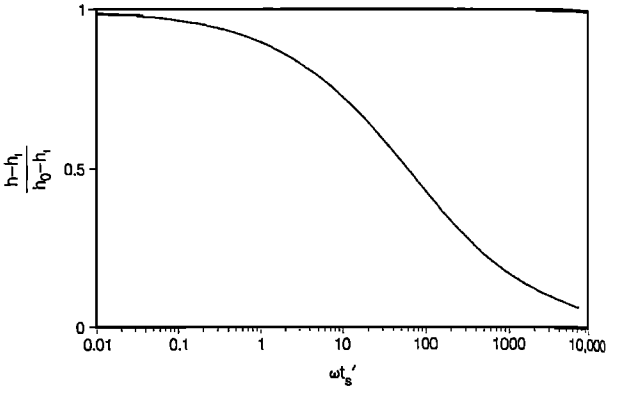

Fig. 3. Type curve for linear flow.

formation may be characterized by one-dimensional flow into the plane of the fracture (Figure 2*a*), where the cross-sectional area available to flow stays constant. One-dimensional flow can also occur when the well intersects a vertical fracture (Figure 2*b*) or there is a prevalent channeling within the fracture (Figure 2*c*).

The slug test problem under these conditions assuming a fracture of infinite lateral extent can be described by

$$\frac{\partial^2 h}{\partial x^2} = \frac{1}{\alpha}\frac{\partial h}{\partial t} \tag{9}$$

where α is the hydraulic diffusivity, with boundary and initial conditions

$$kA\frac{\partial h}{\partial x} = C_w\frac{dh_w}{dt} \qquad x = 0+,\ t > 0 \tag{10}$$

$$h(\infty, t) = h_i \tag{11}$$

$$h(+0, t) = h_w(t) \tag{12}$$

$$h(x, 0) = h_i \tag{13}$$

$$h_w(0) = h_0 \tag{14}$$

The constant A in (10) describes the area open to flow. The above equations in dimensionless forms are

$$\partial^2 h_s/\partial x_D{}^2 = \omega\ \partial h_s/\partial t_s' \tag{15}$$

$$\partial h_s/\partial x_D = dh_{w_s}(t_D)/dt_s' \qquad x_D = 0+ \tag{16}$$

$$h_s(\infty, t_s') = 0 \tag{17}$$

$$h_s(+0, t_s') = h_{w_s}(t_s') \qquad t_s' > 0 \tag{18}$$

$$h_s(x_D, 0) = 0 \tag{19}$$

$$h_{w_s}(0) = 1 \tag{20}$$

where the dimensionless terms are defined as

$$x_D = x/r_w \tag{21}$$

$$t_s' = kAt/r_wC_w \tag{22}$$

$$\omega = Ar_wS_s/C_w \tag{23}$$

The solution to the (15) can be found in the work by *Carslaw and Jaeger* [1946] for an analogous problem of heat transfer and can be written as

$$h_s = e^{\omega x_D + \omega t_s'}\ \text{erfc}\left\{\frac{(\omega)^{1/2}x_D}{2(t_s')^{1/2}} + (\omega t_s')^{1/2}\right\} \tag{24}$$

For $x_D = 0+$, or at the well, (24) simplifies to

$$h_D = (h - h_i)/(h_0 - h_i) = e^{\omega t_s'}\ \text{erfc}\ (\omega t_s')^{1/2} \tag{25}$$

h_w/h_0 versus $\omega t_s'$ is plotted in Figure 3. It should be noted that (25) is a function of $\omega t_s'$ only.

By plotting the observed head normalized to the initial head against time and by superimposing the plot onto Figure 3, one would obtain the hydraulic conductivity-specific storage product:

$$kS_s = \frac{C_w{}^2(\omega t_s')_{\text{match}}}{A^2(t)_{\text{match}}} \tag{26}$$

This equation implies that one cannot obtain separate estimates of the hydraulic conductivity and the specific storage, furthermore, it will probably be very difficult to estimate the

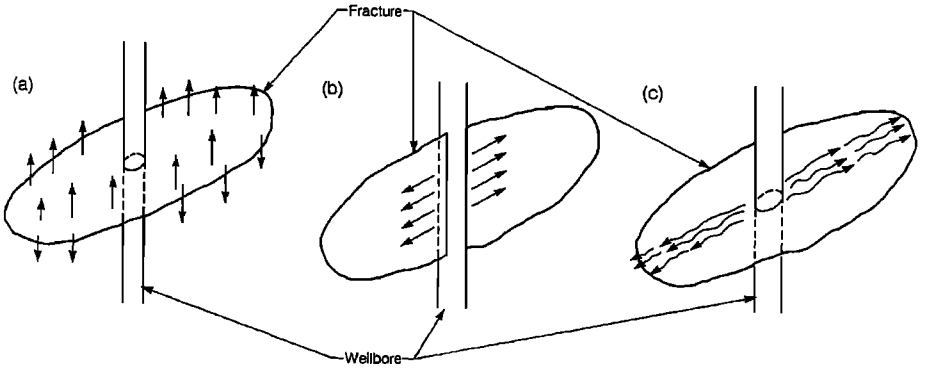

Fig. 2. Possible geometries that cause a linear flow: (*a*) leakage to rock matrix from a very high conductivity fracture, (*b*) flow within a vertical fracture, and (*c*) channelization of flow within a fracture.

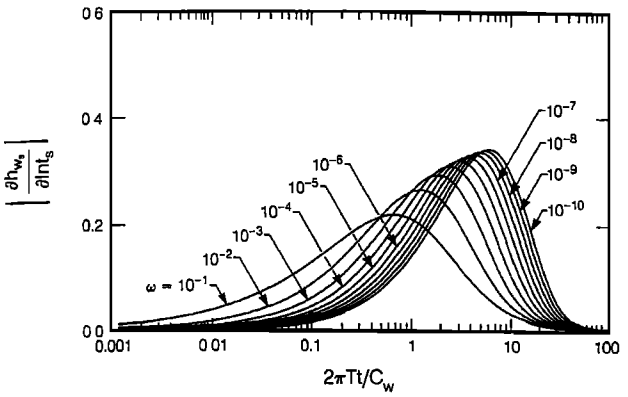

Fig. 4. Derivative plot for *Cooper et al.*'s [1967] model.

value for A. However, the shape of the pressure response plot is distinctively different from those of radial flow type curves for $\omega < 10^{-1}$; i.e., very slow transition (over 6 log cycles) occurs from unity to zero, as can be seen in Figure 3. Therefore if such a slow transition is observed, the presence of a linear flow channel or a large conductivity fracture might be inferred. It must be noted that the type curves for radial flow with large ω ($> 10^{-1}$) could be misapplied to such data.

Derivative Plot Method

Derivative plots have been gaining much attention in the petroleum literature [*Bourdet et al.*, 1983] in the advent of very sensitive downhole instruments. In a derivative plot method, the derivative of the pressure with respect to natural log of time is plotted against time instead of the measured pressure. In this way the rate of pressure change is magnified so that inflection points appear as maxima or minima. Therefore one can sometimes gain more confidence in the type curve match when combined with the usual pressure versus time plot. The derivative plot for *Cooper et al.*'s [1967] solution can be obtained by differentiating (8) with respect to ln t_s:

$$\left|\frac{\partial h_{w_s}(t_s)}{\partial \ln t_s}\right| = \frac{4}{\pi^2}\int_0^\infty e^{-t_s\mu^2/\omega}\frac{\mu t_s\, d\mu}{[\Phi^2(\mu) + \Psi^2(\mu)]} \tag{27}$$

Here the absolute value of the derivative is taken to develop values on a positive abscissa. Equation (27) is evaluated and the resulting plot is shown in Figure 4. As can be seen in the figure, the pressure behavior in the intermediate time range is magnified. The shapes of the curves are more easily distinguished among the different values of ω than is the case in Figure 1. Therefore it may be easier to match the data to a type curve especially when only intermediate time data is available as is the case when slug tests are terminated prematurely due to a time constraint.

Interference Response of a Slug Test

Cooper et al. [1967] presented a solution which describes the pressure response at any point in a reservoir (equation (1)). However, they only evaluated the pressure response at the well (equation (8)). This is because slug tests are ordinarily performed when there is only one well, so that no interference responses are observed. Also, it has been recognized that slug test results reflect the properties of the formation only in the vicinity of the well. As is quoted by *Cooper et al.* [1967], *Ferris et al.* [1962] stated, "the duration of a 'slug' test is very short, hence the estimated transmissivity determined from the test will be representative of only the water-bearing material close to the well." However, this is not quite accurate. The duration of a slug test and the volume covered by the test are not directly related. As can be seen from (3), the duration of a slug test is proportional to the well bore storage and inversely proportional to the transmissivity. The volume of rock that is perturbed by the well test does not depend on the duration of a test but instead it depends on ω, the ratio of formation storativity S to the well storage C_w. Therefore to be useful a slug test may require a long time to complete in a low transmissivity formation, and if the storativity of the formation is large, the results may represent only a small volume of rock. On the other hand, the pressure disturbance could propagate over a fairly large volume of rock if the storativity is very low. Interference responses may therefore be observable in some cases.

The interference responses to a slug test of wells located at $r_D = 10^2$ and 10^3 are shown in Figures 5 (left) and 5 (right), respectively. Figures 6 (left) and 6 (right) are log-log plots of the same curves. From these figures several observations can be made: (1) fairly large responses can be observed at a well located as far as 100 m away for $\omega < 10^{-5}$; (2) in contrast to the responses observed at the injection well, the shapes of the curves are uniquely different from each other even for small values of ω; (3) the transmissivity and storativity can be estimated independently; and (4) a log-log plot enhances the case for a small magnitude response.

Present advances in high-sensitivity pressure transducers may permit interference slug tests even in rocks of moderate storativity. Because it would require no additional instrumentation or significant effort, a slug test may be conducted as a supplement to a constant flux test.

The interference response is calculated based on the assumption that the observation well is infinitesimally thin and has no skin. If this assumption does not hold, the observed responses would be different.

Linear Boundary

The method of images is commonly used to obtain the dimensionless pressure in a reservoir with linear boundaries. However, a simple superposition of the contributions from the image wells onto the dimensionless pressure at the real well alone is not theoretically correct when there is an effect of storage at the real well. This is because the real well acts as an observation well with storage in response to the influence of the image wells. *Tongpenyai and Raghavan* [1981] and *Ogbe and Brigham* [1984] presented a solution for an observation well with well bore storage and skin for a constant flux test. An approach similar to theirs can be taken to obtain the water level in slug tests for the case of a linear boundary. The transient water level at the observation well with the same storage as the injection well is superimposed with the solution for an infinite system. The transient pressure response of an aquifer bounded by a linear constant head boundary located at a distance L/r_w can be expressed in Laplace space as (Appendix A)

$$\bar{h}_{w_s} = \frac{K_0((\omega p)^{1/2})}{pK_0((\omega p)^{1/2}) + (\omega p)^{1/2}K_1((\omega p)^{1/2})} - [(\omega p)^{1/2}K_1((\omega p)^{1/2})K_0((\omega p)^{1/2}2L/r_w)]\{[pK_0((\omega p)^{1/2}) + (\omega p)^{1/2}K_1((\omega p)^{1/2})]^2 - p^2K_0{}^2((\omega p)^{1/2}2L/r_w)\}^{-1} \tag{28}$$

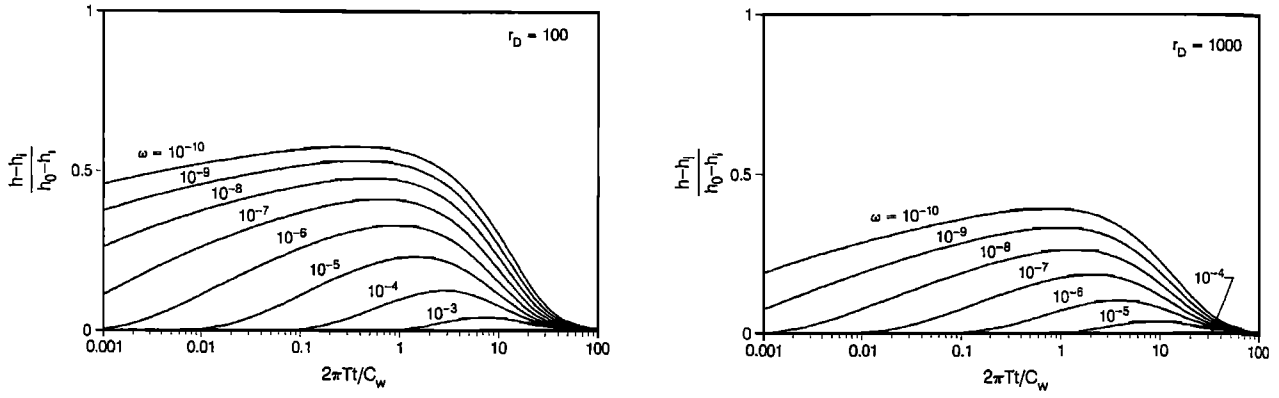

Fig. 5. Interference responses at (left) $r_D = 10^2$ and (right) $r_D = 10^3$.

Equation (28) is numerically inverted back to real space and evaluated for different values of L/r_w and ω. The results are plotted against t_s in Figure 7. As can be seen from the figures, the larger ω and L/r_w are, the smaller the effect of the boundary. However, as ω becomes very small, ($\approx 10^{-9}$), the effect of the boundary can appear even for a large value of L/r_w (= 10^4). Therefore if an open hole slug test is performed in a formation with very low storativity, a boundary as far as 100 m away could be detected.

The boundary effect can be enhanced if a log-log plot of the pressure response curve is used as shown in Figure 8. Note that for an infinite system, the response curve asymptotes to a slope of minus unity. On the other hand, the curves for a formation with a constant head boundary fall sharply below the unit slope near the end of a test. A log-log plot can generally magnify the effects that occur near the end of the slug test. However, for practical reasons, many tests are terminated before the pressure stabilizes.

Radial Constant Head Boundary

The governing equation and the boundary conditions for a system bounded by a circular constant head boundary are the same as those for an infinite system solved by *Cooper et al.* [1967] with the exception of the outer boundary condition. The outer boundary condition is now prescribed at the fixed distance R, i.e.,

$$h_s = 0 \qquad r_D = r_e = R/r_w \tag{29}$$

The solution in the Laplace domain then becomes

$$\bar{h}_s = [-I_0((\omega p)^{1/2}r_e)K_0((\omega p)^{1/2}r_D) + K_0((\omega p)^{1/2}r_e)I_0((\omega p)^{1/2}r_D)]$$
$$\cdot \{K_0((\omega p)^{1/2}r_e)[pI_0((\omega p)^{1/2}) - (\omega p)^{1/2}I_1((\omega p)^{1/2})]$$
$$- I_0((\omega p)^{1/2}r_e)[pK_0((\omega p)^{1/2}) + (\omega p)^{1/2}K_1((\omega p)^{1/2})]\}^{-1} \tag{30}$$

Equation (30) is numerically inverted back to real space. The normalized pressure responses at the injection well with a radial constant head boundary at various dimensionless distances r_e for $\omega = 10^{-4}$ and $\omega = 10^{-9}$ are shown in Figures 9 (left) and 9 (right), respectively. As can be seen from these figures, the boundary is undetectable if ω is larger than 10^{-4} and the dimensionless distance to the boundary r_e is larger than 500. However, for a much smaller value of ω, (10^{-9}), the boundary effect can be felt at as far as $r_e = 10^5$. Unfortunately, the curves are similar enough to each other that it may be difficult to obtain a unique match. If the normalized pressure response is plotted on a log-log scale, the late time behavior of a system with a radial constant head boundary can be distinguished from that of an infinite system because the curve for the radial boundary does not evolve to a straight line with negative unit slope as can be seen in Figure 10.

Layered Aquifer With No Cross Flow

The pressure response of a well penetrating two layers with different flow properties is considered. The model applies to the case where the well intersects large horizontal fractures or faults that are not hydraulically connected except at the well.

The problem can be cast mathematically as follows:

For layer 1

$$\frac{\partial^2 h_1}{\partial r^2} + \frac{1}{r}\frac{\partial h_1}{\partial r} = \frac{1}{\alpha_1}\frac{\partial h_1}{\partial t} \tag{31}$$

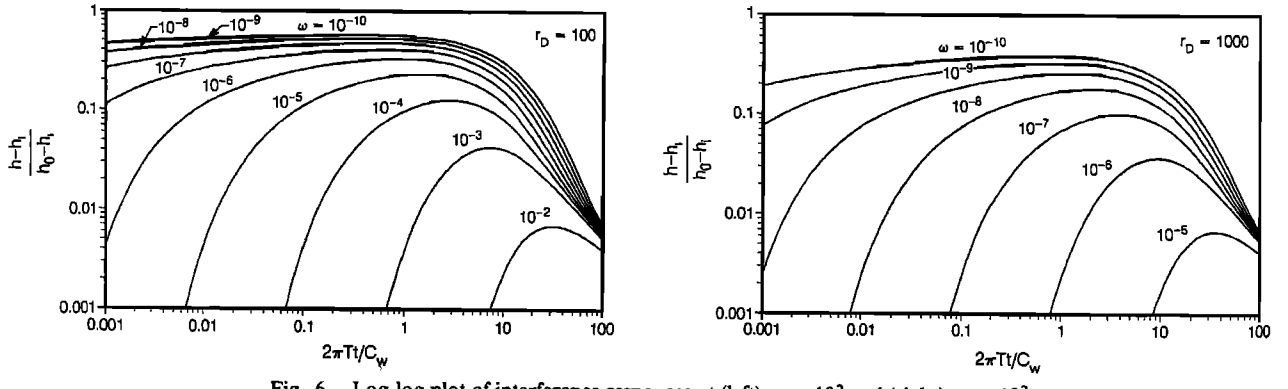

Fig. 6. Log-log plot of interference responses at (left) $r_D = 10^2$ and (right) $r_D = 10^3$.

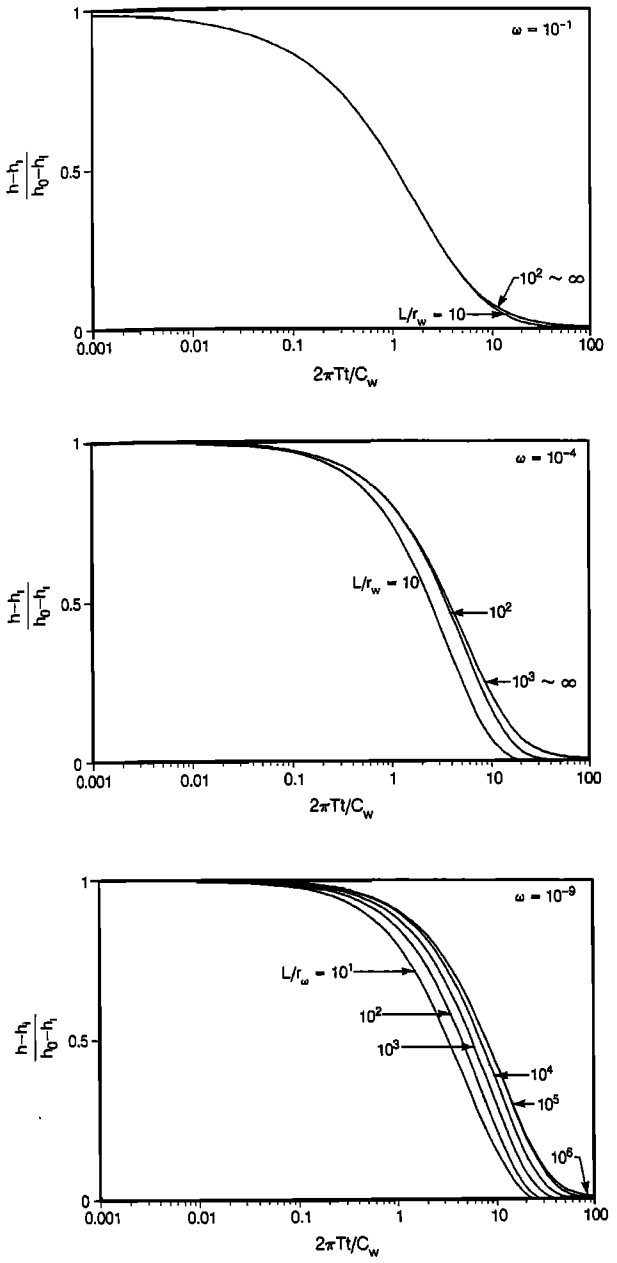

Fig. 7. Effects of linear constant head boundary for (top) $\omega = 10^{-1}$, (middle) $\omega = 10^{-4}$, and (bottom) $\omega = 10^{-9}$.

For layer 2

$$\frac{\partial^2 h_2}{\partial r^2} + \frac{1}{r}\frac{\partial h_2}{\partial r} = \frac{1}{\alpha_2}\frac{\partial h_1}{\partial t} \tag{32}$$

The boundary and initial conditions are

$$2\pi r_w T_1 \frac{\partial h_1}{\partial r} + 2\pi r_w T_2 \frac{\partial h_2}{\partial r} = \pi {r_a}^2 \frac{dh_w}{dt} \qquad r = r_w \tag{33}$$

$$h_1(\infty, t) = 0 \tag{34}$$

$$h_2(\infty, t) = 0 \tag{35}$$

$$h_1(r_w + 0, t) = h_2(r_w + 0, t) = h_w(t) \qquad t > 0 \tag{36}$$

$$h_1(r, 0) = h_2(r, 0) = 0 \tag{37}$$

$$h_w(0) = h_0 \tag{38}$$

Casting (31) through (38) in dimensionless form we obtain

$$\frac{\partial^2 h_{s_1}}{\partial {r_D}^2} + \frac{1}{r_D}\frac{\partial h_{s_1}}{\partial r_D} = \omega \frac{\partial h_{s_1}}{\partial t_D} \tag{39}$$

$$\frac{\partial^2 h_{s_2}}{\partial {r_D}^2} + \frac{1}{r_D}\frac{\partial h_{s_2}}{\partial r_D} = \frac{\omega}{\alpha_c}\frac{\partial h_{s_2}}{\partial t_D} \tag{40}$$

$$\frac{\partial h_{s_1}}{\partial r_D} + \beta \frac{\partial h_{s_2}}{\partial r_D} = \frac{dh_{w_s}}{dt_D} \qquad r_D = 1 \tag{41}$$

$$h_{s_1}(\infty, t_D) = 0 \tag{42}$$

$$h_{s_2}(\infty, t_D) = 0 \tag{43}$$

$$h_{s_1}(1 + 0, t_D) = h_{s_2}(1 + 0, t_D) = h_{w_s}(t_D) \qquad t_D > 0 \tag{44}$$

$$h_{s_1}(r_D, 0) = h_{s_2}(r_D, 0) = 0 \tag{45}$$

$$h_w(0) = 1 \tag{46}$$

where $\beta = T_2/T_1$, $\alpha_c = \alpha_2/\alpha_1 = \beta/\gamma$, and $\gamma = S_2/S_1$.

The solution in Laplace space at $r_D = 1$ is found to be

$$\bar{h}_{s_1}(1) = \bar{h}_{s_2}(1) = K_0((\omega p)^{1/2})K_0((\omega p/\alpha_c)^{1/2}) \cdot [pK_0((\omega p)^{1/2})K_0((\omega p/\alpha_c)^{1/2}) + (\omega p)^{1/2}K_1((\omega p)^{1/2})K_0((\omega p/\alpha_c)^{1/2}) + \beta((\omega p/\alpha_c)^{1/2})K_0((\omega p)^{1/2})K_1((\omega p/\alpha_c)^{1/2})]^{-1} \tag{47}$$

Equation (47) is again inverted back to the real space using the algorithm introduced by *Stehfest* [1970]. Figures 11 (left) and 11 (right) show the normalized pressure responses when ω of one of the layers is 10^{-4} and 10^{-9}, respectively. The curves are plotted for different values of β and γ. From these figures, the following observations are pertinent. The behavior of a two-layer system is similar to that of one-layer system with the equivalent transmissivity equal to the arithmetic sum of the two. The dimensionless storage ω obtained by analyzing a two-layer system is nearly equal to that of the ω value of the layer with the larger transmissivity if $\beta \gg 1$ or $\beta \ll 1$. For $\beta \approx 1$, ω is the arithmetic average of the two ω values. Therefore it is probably impossible to distinguish a two-layer system from a one-layer system. This should hold for multiple-layered systems of more than two layers. A similar conclusion has been made for constant flux tests [*Lefkovits et al.*, 1961; *Russell and Prats*, 1962].

Linear Radial Flow Model

The presence of natural fractures complicates the interpretation of well tests. One of the reasons for this is that the flow near the well is mainly controlled by the fractures intersecting the well and, depending on the geometry of the fractures, may represent a different flow regime from that of the system as a whole. For this reason the standard radial flow solutions are sometimes inadequate in analyzing well test data for a well intercepting fractures. If there is only a small number of fractures intersecting the injection well, the single continuum approximation may not be appropriate because the properties and the geometries of these few fractures may control flow in the vicinity of the well. Therefore the characteristics of fractures close to the well must be accounted for, especially if the hydraulic parameters of these fractures are significantly different from the average values for the entire system.

When a well intercepts a few vertical fractures or when the flow near the well is restricted to be entirely within channels in the fractures of any orientation, the flow near the well may be more linear than radial; that is, the cross-sectional area avail-

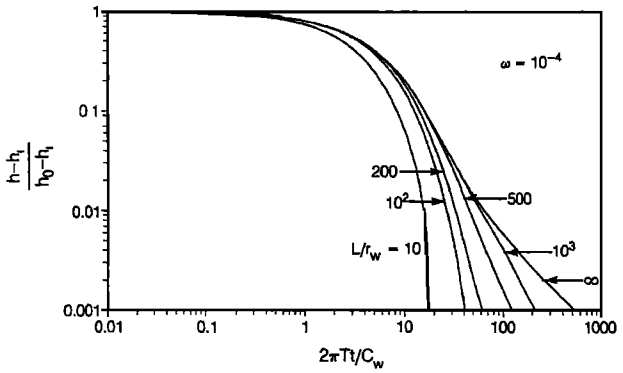

Fig. 8. Log-log plot of Figure 7b.

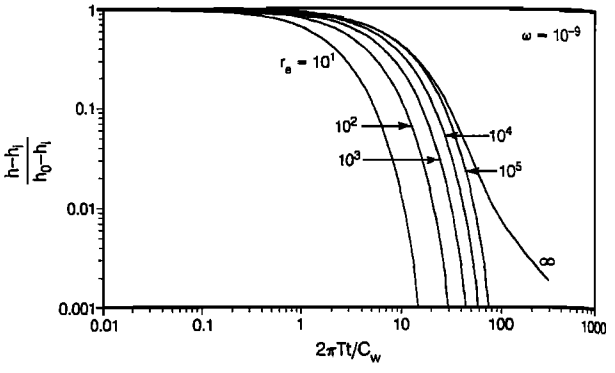

Fig. 10. Log-log plot for $\omega = 10^{-9}$.

able to flow does not change with the radial distance. In such cases, the system can be described by a concentric composite model, in which the flow is assumed to be linear in the inner region and radial in the outer region. The proposed analytical model is a composite system with two concentric regions. The inner region is composed of a finite number of fractures whose flow characteristics and properties are different from the average values for the entire system. In the outer region it is assumed that the flow takes place in a sufficient number of fractures so that the flow is, on the average, radial and that the classical porous medium approximation applies. The model is similar to the problem discussed by *Karasaki et al.* [1988] for constant rate pumping test. In the present paper, the problem is solved for slug test conditions.

The governing equations for the inner and outer regions are

$$\frac{\partial^2 h_1}{\partial r^2} = \frac{1}{\alpha_1}\frac{\partial h_1}{\partial t} \tag{48}$$

$$\frac{\partial^2 h_2}{\partial r^2} + \frac{1}{r}\frac{\partial h_2}{\partial r} = \frac{1}{\alpha_2}\frac{\partial h_2}{\partial t} \tag{49}$$

The inner boundary condition is one that involves a time derivative:

$$nk_1 bH \left.\frac{\partial h_1}{\partial r}\right|_{r=r_w+0} = C_w \frac{dh_w}{dt} \tag{50}$$

where $C_w = \pi r_a^2$ for an open well test whose casing radius is r_a, in which the water level h_w changes, and the relation between h_1 and h_w is

$$h_1(r_{w+0}, t) = h_w(t) \tag{51}$$

The outer boundary condition is that for a infinite medium:

$$h_2(\infty, t) = h_i \tag{52}$$

The initial conditions are

$$h_w(0) = h_0 \tag{53}$$

$$h_1(r, 0) = h_i \qquad r_w < r \le r_f \tag{54}$$

$$h_2(r, 0) = h_i \qquad r_f \le r \le \infty \tag{55}$$

The continuity requirements at the interface of the inner and outer regions are as follows:

$$h_1 = h_2 \qquad r = r_f \tag{56}$$

$$nk_1 b \frac{\partial h_1}{\partial r} = 2\pi r_f k_2 \frac{\partial h_2}{\partial r} \qquad r = r_f \tag{57}$$

Dimensionless parameters are defined as

$$h_s = (h - h_i)/(h_0 - h_i) \tag{58}$$

$$t_D = \frac{2\pi T_2 t}{C_w}\frac{1}{\omega} = \frac{2\pi T_2 t}{C_w}\frac{C_w}{2\pi {r_f}^2 S_2} = \frac{\alpha_2 t}{{r_f}^2} \tag{59}$$

$$r_D = r/r_f \tag{60}$$

$$r_c = r_w/r_f \tag{61}$$

$$\alpha_c = \alpha_1/\alpha_2 \tag{62}$$

$$\beta = nk_1 b/2\pi r_f k_2 \tag{63}$$

$$\omega = (2\pi {r_f}^2/C_w)S_2 \tag{64}$$

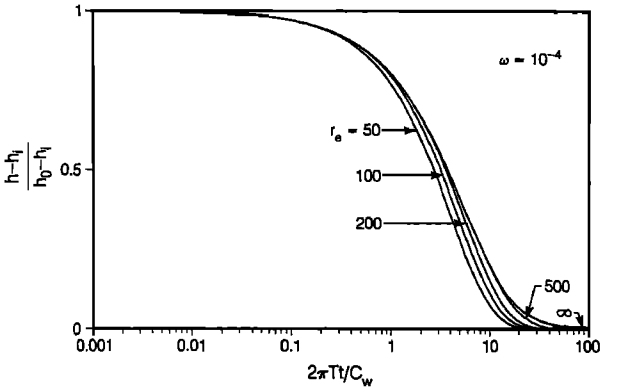

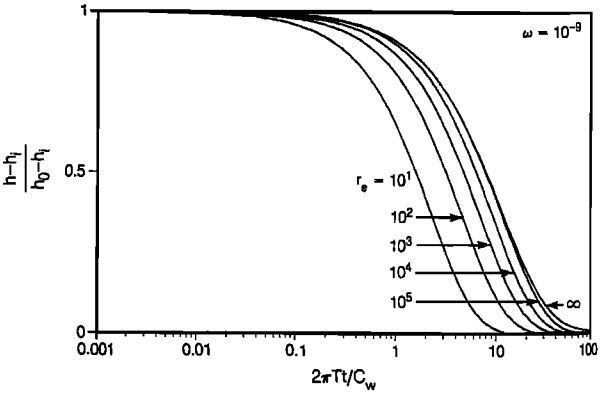

Fig. 9. Responses to a radial constant head boundary for (left) $\omega = 10^{-4}$ and (right) $\omega = 10^{-9}$.

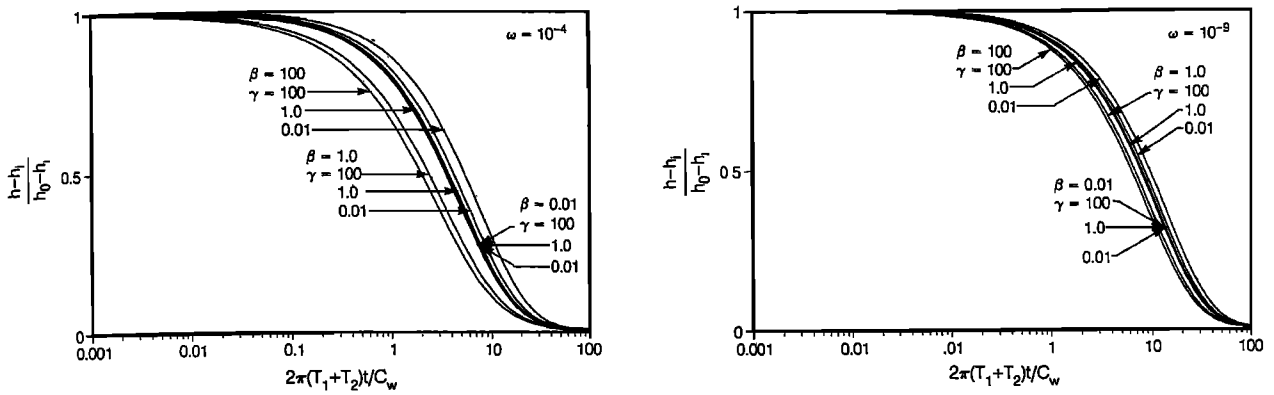

Fig. 11. Response of a two-layered aquifer for (left) $\omega = 10^{-4}$ and (right) $\omega = 10^{-9}$.

Therefore the governing equations in dimensionless form become

$$\frac{\partial^2 h_{s_1}}{\partial r_D^2} = \frac{1}{\alpha_c}\frac{\partial h_{s_1}}{\partial t_D} \tag{65}$$

$$\frac{\partial^2 h_{s_2}}{\partial r_D^2} + \frac{1}{r_D}\frac{\partial h_{s_2}}{\partial r_D} = \frac{\partial h_{s_1}}{\partial t_D} \tag{66}$$

The boundary, initial, and interface conditions corresponding to (50) through (57) are now

$$\frac{\partial h_{s_1}}{\partial r_D} = \frac{1}{\omega\beta}\frac{dh_{ws}}{dt_D} \qquad r_D = r_c \tag{67}$$

$$h_{s_1}(r_{c+0}, t_D) = h_{ws}(t_D) \tag{68}$$

$$h_{s_2}(\infty, t_D) = 0 \tag{69}$$

$$h_{ws}(0) = 1 \tag{70}$$

$$h_{s_1}(r_D, 0) = 0 \qquad r_C < r_D \le 1 \tag{71}$$

$$h_{s_2}(r_D, 0) = 0 \qquad 1 \le r_D \le \infty \tag{72}$$

$$h_{s_1} = h_{s_2} \qquad r_D = 1 \tag{73}$$

$$\frac{\partial h_{s_1}}{\partial r_D} = \frac{1}{\beta}\frac{\partial h_{s_2}}{\partial r_D} \qquad r_D = 1 \tag{74}$$

The solutions in the Laplace domain can be written as (Appendix B)

$$\bar{h}_{s_1} = \frac{(\alpha_c)^{1/2}}{\beta\sqrt{p}}\frac{1}{\Delta}\{\sqrt{\alpha_c}K_1(\sqrt{p})\sinh[(p/\alpha_c)^{1/2}(1-r_D)] + \beta K_0(\sqrt{p})\cosh[(p/\alpha_c)^{1/2}(1-r_D)]\} \tag{75}$$

for the inner region and

$$\bar{h}_{s_2} = \frac{1}{(p/\alpha_c)^{1/2}\Delta}K_0(\sqrt{p}r_D) \tag{76}$$

for the outer region, where

$$\Delta = \sqrt{\alpha_c}[\omega K_1(\sqrt{p}) + \sqrt{p}K_0(\sqrt{p})]\cosh(p/\alpha_c)^{1/2}(1-r_c) + \beta\left[\frac{\alpha_c}{\beta^2}\sqrt{p}K_1(\sqrt{p}) + \omega K_0(\sqrt{p})\right]\sinh(p/\alpha_c)^{1/2}(1-r_c) \tag{77}$$

To obtain the normalized head at the well, (75) is numerically inverted back to real space and evaluated at $r_D = r_c$ for various values of α_c, β, and ω. Figure 12 shows the particular cases of $r_c = 0.005$ for $\omega = 10^{-3}$, 10^{-4}, and 10^{-9}, respectively. Note a new dimensionless time nbT_1t/C_wr_w, and a new storage ratio $w' = nbr_wS_1/C_w$, that are based on the inner region transmissivity and storativity, are used in plotting these curves. The curves show the effects of changes in the flow properties from the inner to the outer region.

A composite medium behavior is noticeable only when the contribution of the infinite acting period of the inner region on the head change is significant but does not account for all the change (Figure 12 (top)). When the transmissivity of the outer region is small compared to that of the inner region (large values of β), the curves display two staged decline. The point of deflection moves to later time as r_c increases. For values of β smaller than 10^{-2}, i.e., when the outer region transmissivity is large compared to that of the inner region, the curves are identical to each other and essentially present the effect of an open boundary.

When the total storage capacity of the inner region is very small, the curves appear to be merely shifted horizontally to the left or right depending on the hydraulic conductivity contrast β (Figure 12 (bottom)). Although the shapes of the curves are different from each other, the differences are minute and may not be distinguishable. The smaller the diameter of the inner region and the smaller the storage coefficient of the inner region, the smaller the total storage capacity. Conversely, if the total storage capacity of the inner region is large, the inner region would be infinite acting and the effect of the outer region would not be observed. For all cases except in Figure 12 (top), it is assumed that $\alpha_c/\beta = 1$. In Figure 12 (top), curves for $\alpha_c/\beta = 0.1$ and 10 when $\beta = 10^{-2}$ are also shown but the effect of different values of α_c/β is insignificant for the particular case.

Spherical Flow Model

When the length of a well open to flow is much smaller than the thickness of the formation and when the vertical hydraulic conductivity is comparable to the horizontal hydraulic conductivity, the flow may be better approximated by spherical flow. The governing equation for spherical flow can be written as

$$\frac{\partial^2 h}{\partial r^2} + \frac{2}{r}\frac{\partial h}{\partial r} = \frac{1}{\alpha}\frac{\partial h}{\partial t} \tag{78}$$

The initial conditions are

$$h(r, 0) = 0 \tag{79}$$

$$h(r_w + 0, t) = h_w(t) \tag{80}$$

$$h_w(0) = h_0 \tag{81}$$

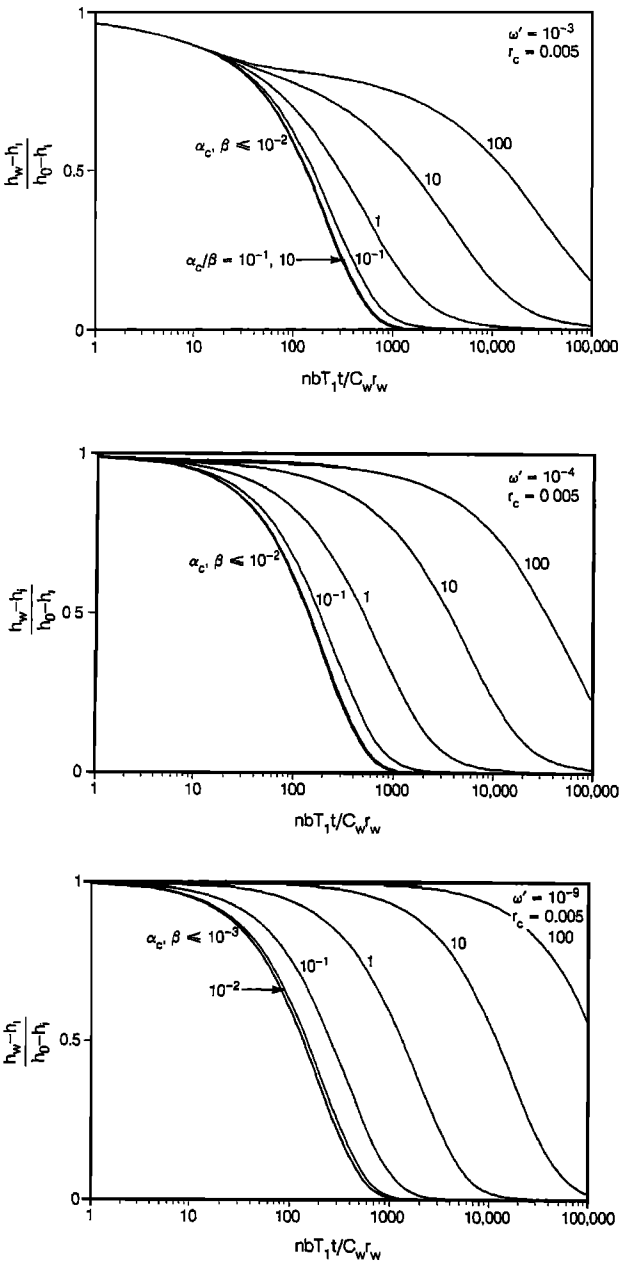

Fig. 12. Normalized head for linear-radial model (top) $\omega' = 10^{-3}$, (middle) $\omega' = 10^{-4}$, and (bottom) $\omega' = 10^{-9}$.

The boundary conditions are

$$4\pi r_w^2 k \left.\frac{\partial h}{\partial r}\right|_{r=r_w} = C_w \frac{dh_w}{dt} \tag{82}$$

$$h(\infty, t) = 0 \tag{83}$$

In dimensionless form, they become

$$\frac{\partial^2 h_s}{\partial r_D^2} + \frac{2}{r_D}\frac{\partial h_s}{\partial h_D} = \omega \frac{\partial h_s}{\partial t_s} \tag{84}$$

$$h_s(r_D, 0) = 0 \tag{85}$$

$$h_s(1 + 0, t_s) = h_{w_s}(t_s) \tag{86}$$

$$\left.\frac{\partial h_s}{\partial r_D}\right|_{r_D=1} = \frac{dh_{w_s}}{dt_s} \tag{87}$$

$$h_s(\infty, t_s) = 0 \tag{88}$$

$$h_{w_s}(0) = 1 \tag{89}$$

with the following definitions for t_s and ω:

$$t_s = 4\pi r_w kt/C_w \tag{90}$$

$$\omega = 4\pi r_w^3 S_s/C_w \tag{91}$$

The solution can be found by *Carslaw and Jaeger* [1946] for the analogous problem in heat flow. The normalized water level in the well is

$$h_s = \frac{2\omega}{\pi}\int_0^\infty \frac{e^{-t_s\mu^2/\omega}\mu^2}{(\mu^2-\omega)^2 + \omega^2\mu^2}\, d\mu \tag{92}$$

Equation (92) is evaluated for a wide range of values of ω ($10^{-10} \le \omega < 10$) and the resulting normalized fluid levels at the well are shown in Figure 13. It can be seen that the transition of the fluid level from unity to zero occurs much faster and the fluid level diminishes to zero more abruptly than when the flow is radial. Therefore if a test result shows such characteristics, spherical flow can be suspected. However, the curves for the values of ω smaller than 10^{-3} are indistinguishable from each other. Therefore it will not be possible to estimate the storage coefficient values smaller than 10^{-3}. For a system with a larger value of ω, the volume of the rock tested would be so small that the reliability of the estimated storage coefficient value would be questionable.

RADIAL-SPHERICAL COMPOSITE MODEL

We will now consider a problem where a well intersects a subhorizontal fracture that is part of an interconnected fracture system. We assume that the flow near the wellbore is radial and at some distance from the well the flow becomes spherical. We also assume that the fracture and the wellbore intersection is circular. This is not exact when the fracture intersects the well bore at some oblique angle because the intersection is an ellipse. However, the error may not be very large since the flow becomes near radial for large r/r_w. The governing equations for this composite system are

$$\frac{\partial^2 h_1}{\partial r^2} + \frac{1}{r}\frac{\partial h_1}{\partial r} = \frac{1}{\alpha_1}\frac{\partial h_1}{\partial t} \tag{93}$$

$$\frac{\partial^2 h_2}{\partial r^2} + \frac{2}{r}\frac{\partial h_2}{\partial r} = \frac{1}{\alpha_2}\frac{\partial h_2}{\partial t} \tag{94}$$

These equations will be solved under the following boundary conditions. The inner boundary condition is now expressed as follows:

$$2\pi r_w b k_1 \left.\frac{\partial h_1}{\partial r}\right|_{r=r_w} = C_w \frac{dh_w}{dt} = C_w \frac{\partial h_1}{\partial t} \qquad r = r_w \tag{95}$$

The outer boundary condition is that for a infinite medium

$$h_2(\infty, t) = h_i \tag{96}$$

The initial conditions are

$$h_w(0) = h_0 \tag{97}$$

$$h_1(r, 0) = h_i \qquad r_w < r \le r_f \tag{98}$$

$$h_2(r, 0) = h_i \qquad r_f \le r \le \infty \tag{99}$$

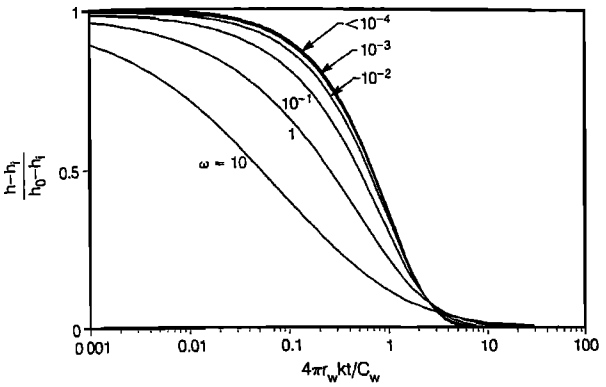

Fig. 13. Normalized head for spherical flow model.

The continuity requirements at the interface of the inner and outer regions are as follows:

$$h_1 = h_2 \qquad r = r_f \tag{100}$$

$$2\pi r_f b k_1 \frac{\partial h_1}{\partial r} = 4\pi {r_f}^2 k_2 \frac{\partial h_2}{\partial r} \qquad r = r_f \tag{101}$$

Dimensionless parameters are defined as

$$h_s = (h - h_i)/(h_0 - h_i) \tag{102}$$

$$t_D = \frac{2\pi T_2 t}{C_w}\frac{1}{\omega} = \frac{2\pi T_2 t}{C_w}\frac{C_w}{2\pi {r_f}^2 S_2} = \frac{\alpha_2 t}{{r_f}^2} \tag{103}$$

$$r_D = r/r_f \tag{104}$$

$$r_c = r_w/r_f \tag{105}$$

$$\alpha_c = \alpha_1/\alpha_2 \tag{106}$$

$$\beta = bk_1/2r_f k_2 \tag{107}$$

$$\omega = \frac{4\pi {r_f}^2 r_w}{C_w} S_{s_2} \tag{108}$$

In dimensionless form the governing equations become

$$\frac{\partial^2 h_{s_1}}{\partial {r_D}^2} + \frac{1}{r_D}\frac{\partial h_{s_1}}{\partial r_D} = \frac{1}{\alpha_c}\frac{\partial h_{s_1}}{\partial t_D} \tag{109}$$

$$\frac{\partial^2 h_{s_2}}{\partial {r_D}^2} + \frac{2}{r_D}\frac{\partial h_{s_2}}{\partial r_D} = \frac{\partial h_{s_2}}{\partial t_D} \tag{110}$$

The boundary conditions are now identical to (67) through (74). The Laplace space solution for the inner region ($r_c \le r_D \le 1$) becomes

$$\bar{h}_{s_1} = \frac{1}{\omega\beta\Delta}\left[\frac{1+\sqrt{p}}{\beta} K_0((p/\alpha_c)^{1/2}) - (p/\alpha_c)^{1/2} K_1((p/\alpha_c)^{1/2})\right] \cdot I_0((p/\alpha_c)^{1/2} r_D) - \left[\frac{1+\sqrt{p}}{\beta} I_0((p/\alpha_c)^{1/2}) + (p/\alpha_c)^{1/2} I_1((p/\alpha_c)^{1/2})\right] K_0((p/\alpha_c)^{1/2} r_D) \tag{111}$$

where

$$\Delta = \left[-(p/\alpha_c)^{1/2} I_1((p/\alpha_c)^{1/2} r_c + \frac{p}{\omega\beta} I_0((p/\alpha_c)^{1/2} r_c)\right] \cdot \left[\frac{1+\sqrt{p}}{\beta} K_0((p/\alpha_c)^{1/2}) - (p/\alpha_c)^{1/2} K_1((p/\alpha_c)^{1/2})\right] - \left[(p/\alpha_c)^{1/2} K_1((p/\alpha_c)^{1/2} r_c) + \frac{p}{\omega\beta} K_0((p/\alpha_c)^{1/2} r_c)\right] \cdot \left[\frac{1+\sqrt{p}}{\beta} I_0((p/\alpha_c)^{1/2}) + (p/\alpha_c)^{1/2} I_1((p/\alpha_c)^{1/2})\right] \tag{112}$$

and for completeness, the outer region solution ($r_D \ge 1$) is

$$\bar{h}_{s_2} = -\frac{\exp\left[-\sqrt{p}(r_D - 1)\right]}{r_D \omega\beta\Delta} \tag{113}$$

The normalized head at the well can be obtained by numerically inverting (111) back to the real space and evaluating at $r_D = r_c$ for various values of α_c, β, and ω. Figures 14 (left) and 14 (right) show the particular case of $r_c = 0.02$ for values of $\omega = 10^{-3}$ and 10^{-6}, respectively. Note that a new dimensionless time $2\pi b k_1 t/C_w$, and a new dimensionless storage ratio $2\pi b r_w S_{s_1}/C_w$, have been used in developing these curves.

Similar observations as in the linear-radial flow model can be made on these figures. The curves show the effects of the change in the flow properties from the inner to the outer region. A composite medium behavior is noticeable only when the contribution of the infinite acting period of the inner region on the head change is significant but does not account for all the change (Figure 14 (left)). The early time behavior is that of radial flow with its shape reflecting the ω' value. However, unlike the constant flux case [*Karasaki*, 1986], the late time behavior does not reflect the obvious characteristics of spherical flow. When the transmissivity of the outer region is small compared to that of the inner region (large values of β), the curves display a two-stage decline. It can be shown that as r_c increases, the point of deflection moves to later time. For values of β smaller than 10^{-2}, i.e., large outer region transmissivity compared to that of the inner region, the curves are identical to each other and essentially present the same effect as an open boundary.

When the total storage capacity of the inner region is very small, the curves appear to be merely shifted horizontally to the left or right, depending on the hydraulic conductivity contrast β (Figure 14 (right)). The smaller the diameter and storage coefficient of the inner region, the smaller the total storage capacity of the inner region. The shift to the left is bounded by the curve for $\beta = 0.1$. The curves for $\beta < 0.1$ are virtually indistinguishable from each other. Although the shapes of the other curves are different from each other, the differences are small, and it may be difficult to determine which type curve to use in matching field data. Conversely, if the total storage capacity of the inner region is large, the inner region would be infinite acting and the effect of the outer region would not be observed. In this case, one can use a homogeneous radial flow model. For the cases in Figure 14, it is assumed that $\alpha_c/\beta = 1$. It can be shown but the effect of different values of α_c/β is insignificant.

CONCLUSIONS

In the present paper, several solutions that may be used for analyzing slug tests were presented. The geometric conditions that may be present in fractured media were considered, although these conditions are not limited to such media. The type curves developed for each model can be used to estimate such geometric parameters as the distance to the boundary as well as the flow parameters. However, analyses of slug test results suffer problems of nonuniqueness, more than other well

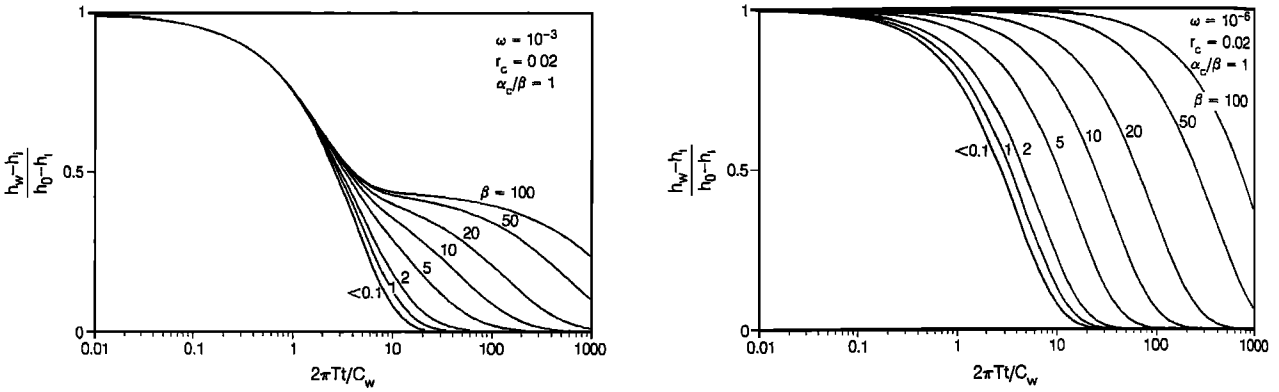

Fig. 14. Normalized head for radial-spherical model: (left) $\omega' = 10^{-3}$ and (right) $\omega' = 10^{-6}$.

tests. As can be seen from the figures presented, many curves have unique shapes only for some combination of the flow parameters and distance. Other sets of type curves are all similar in shape, although log-log plots may emphasize some features that may not be apparent in semilog plots. Therefore it is important that one consider all other available information, such as geology and geophysical data, when analyzing results of slug tests. We recommend that the analysis of slug test results be carried out in the following steps: (1) review existing borehole and surrounding geologic information and build a conceptual model of the test geometry, (2) review previous hydrologic testing for indications of existing test system conditions, (3) plot slug test response data in log-log and semilog form using traditional and pressure derivative methods for diagnostic identification of the operative conceptual model, (4) find or generate appropriate type curves for the conceptual model, and (5) curve match to obtain system parameters. Because of the nonuniqueness problem, authors recommend against using slug tests alone to estimate flow parameters in heterogeneous media such as fractured rocks.

Appendix A: Solution Scheme for Linear Boundary

The transient water level with a linear boundary located at L/r_w can be obtained by superimposing the influence of the image well located at $2L/r_w$ on the water level in an infinite system, h_{im}, the water level change due to the image well can be obtained following the similar steps as *Ogbe and Brigham* [1984]. By denoting the real well by subscript 1 and the image well by subscript 2, the general solution in Laplace space can be written as

$$\bar{h}_{im} = C_1 K_0((\omega p)^{1/2} r_{D_1}) + C_2 K_0((\omega p)^{1/2} r_{D_2}) \tag{A1}$$

where C_1 and C_2 are arbitrary constants. At the real well, i.e., $r_{D_1} = 1$ and $r_{D_2} \approx 2L/r_w$, the boundary condition can be written as

$$\partial \bar{h}_{im}/\partial r_{D_1} = p\bar{h}_{im} \tag{A2}$$

and at the image well, i.e., at $r_{D_1} \approx 2L/r_w$ and $r_{D_2} = 1$, it is

$$\partial \bar{h}_{im}/\partial r_{D_1} = p\bar{h}_{im} - 1 \tag{A3}$$

Using the boundary conditions in (A2) and (A3), we can solve for C_1 and C_2

$$C_1 = -[pK_0((\omega p)^{1/2} 2L/r_w)]\{[pK_0((\omega p)^{1/2}) + (\omega p)^{1/2} K_1((\omega p)^{1/2})]^2 - p^2 K_0{}^2((\omega p)^{1/2} 2L/r_w)\}^{-1} \tag{A4}$$

$$C_2 = \{[pK_0((\omega p)^{1/2}) + (\omega p)^{1/2} K_1((\omega p)^{1/2})]\}\{[pK_0((\omega p)^{1/2}) + (\omega p)^{1/2} K_1((\omega p)^{1/2})]^2 - p^2 K_0{}^2((\omega p)^{1/2} 2L/r_w)\}^{-1} \tag{A5}$$

so that

$$\bar{h}_{im} = \{pK_0((\omega p)^{1/2} 2L/r_w) K_0((\omega p)^{1/2} r_{D_1}) + [pK_0((\omega p)^{1/2}) + (\omega p)^{1/2} K_1((\omega p)^{1/2})] K_0((\omega p)^{1/2} r_{D_2})\} \cdot \{[pK_0((\omega p)^{1/2}) + (\omega p)^{1/2} K_1((\omega p)^{1/2})]^2 - p^2 K_0{}^2((\omega p)^{1/2} 2L/r_w)\}^{-1} \tag{A6}$$

Therefore the normalized water level due to the image well as observed at the real well, i.e., $r_{D_1} = 1$, $r_{D_2} \approx 2L/r_w$ is

$$\bar{h}_{im} = [(\omega p)^{1/2} K_1((\omega p)^{1/2}) K_0((\omega p)^{1/2} 2L/r_w)]\{[pK_0((\omega p)^{1/2}) + (\omega p)^{1/2} K_1((\omega p)^{1/2})]^2 - p^2 K_0{}^2((\omega p)^{1/2} 2L/r_w)\}^{-1} \tag{A7}$$

Finally, the water level at the injection well can be obtained by a superposition.

Appendix B: Solution Scheme for Linear Radial Flow Model

The Laplace transformation of the governing (65) and (66) with the initial conditions in (71) and (72) yield the following subsidiary equations:

$$\frac{d^2 \bar{h}_{s_1}}{dr_D{}^2} = \frac{p}{\alpha_c} \bar{h}_{s_1} \tag{B1}$$

$$\frac{d^2 \bar{h}_{s_2}}{dr_D{}^2} + \frac{1}{r_D} \frac{d\bar{h}_{s_2}}{dr_D} = p\bar{h}_{s_2} \tag{B2}$$

The transformed boundary and interface conditions are

$$\frac{d\bar{h}_{s_1}}{dr_D} = \frac{1}{\omega\beta} [p\bar{h}_{s_1} - 1] \qquad r_D = r_c \tag{B3}$$

$$\bar{h}_{s_2}(\infty, t_D) = 0 \tag{B4}$$

$$\bar{h}_{s_1} = \bar{h}_{s_2} \qquad r_D = 1 \tag{B5}$$

$$\frac{d\bar{h}_{s_1}}{dr_D} = \frac{1}{\beta} \frac{d\bar{h}_{s_2}}{dr_D} \qquad r_D = 1 \tag{B6}$$

The general solutions to the (B1) and (B2) are

$$\bar{h}_{s_1} = A \cosh((p/\alpha_c)^{1/2} r_D) + B \sinh((p/\alpha_c)^{1/2} r_D) \tag{B7}$$

$$\bar{h}_{s_2} = CI_0(\sqrt{p} r_D) + DK_0(\sqrt{p} r_D) \tag{B8}$$

Equation (B4) requires the solution to be bounded so that $C = 0$ in (B8). Applying the boundary conditions in (B3), (B5), and (B6) we obtain

$$A(p/\alpha_c)^{1/2} \sinh ((p/\alpha_c)^{1/2} r_c) + B(p/\alpha_c)^{1/2} \cosh ((p/\alpha_c)^{1/2} r_c) = \frac{1}{\omega\beta} \{p[A \cosh ((p/\alpha_c)^{1/2} r_c) + B \sinh ((p/\alpha_c)^{1/2} r_c)] - 1\} \quad \text{(B9)}$$

$$A \cosh (p/\alpha_c)^{1/2} + B \sinh (p/\alpha_c)^{1/2} = DK_0(\sqrt{p}) \quad \text{(B10)}$$

$$A(p/\alpha_c)^{1/2} \sinh (p/\alpha_c)^{1/2} + B(p/\alpha_c)^{1/2} \cosh (p/\alpha_c)^{1/2} = -\frac{D}{\beta} \sqrt{p} K_1(\sqrt{p}) \quad \text{(B11)}$$

We now solve (B9) through (B11) for A, B, and D. After some manipulation, we obtain

$$A = \frac{(\alpha_c)^{1/2}}{\beta\sqrt{p}\Delta} \{(\alpha_c)^{1/2} K_1(\sqrt{p}) \sinh (p/\alpha_c)^{1/2} + \beta K_0(\sqrt{p}) \cosh (p/\alpha_c)^{1/2}\} \quad \text{(B12)}$$

$$B = \frac{(\alpha_c)^{1/2}}{\beta\sqrt{p}\Delta} \{(\alpha_c)^{1/2} K_1(\sqrt{p}) \cosh (p/\alpha_c)^{1/2} + \beta K_0(\sqrt{p}) \sinh (p/\alpha_c)^{1/2}\} \quad \text{(B13)}$$

$$D = \frac{1}{(p/\alpha_c)^{1/2}\Delta} \quad \text{(B14)}$$

where

$$\Delta = (\alpha_c)^{1/2}[\omega K_1(\sqrt{p}) + \sqrt{p} K_0(\sqrt{p})] \cosh (p/\alpha_c)^{1/2}(1 - r_c) + \beta\left[\frac{\alpha_c}{\beta^2}\sqrt{p} K_1(\sqrt{p}) + \omega K_0(\sqrt{p})\right] \sinh (p/\alpha_c)^{1/2}(1 - r_c) \quad \text{(B15)}$$

Finally, the solutions in the Laplace domain become

$$\bar{h}_{s_1} = \frac{\sqrt{\alpha_c}}{\beta\sqrt{p}} \frac{1}{\Delta} \{(\alpha_c)^{1/2} K_1(\sqrt{p}) \sinh [(p/\alpha_c)^{1/2}(1 - r_D)] + \beta K_0(\sqrt{p}) \cosh [(p/\alpha_c)^{1/2}(1 - r_D)]\} \quad \text{(B16)}$$

for the inner region and

$$\bar{h}_{s_2} = \frac{1}{(p/\alpha_c)^{1/2}\Delta} K_0(\sqrt{p} r_D) \quad \text{(B17)}$$

for the outer region.

NOTATION

- A area of flow, L^2.
- b fracture aperture, L.
- c_w compressibility of water, LT^2/M.
- C_w well bore storage, L^2.
- g acceleration of gravity, L/T^2.
- h hydraulic head, L.
- h_D dimensionless head.
- h_i initial head in formation, L.
- h_s normalized head, $h - h_i/h_0 - h_i$.
- h_w pressure head in well, L.
- h_{w_s} normalized head in well.
- h_0 initial head in well, L.
- H formation thickness, L.
- I_0 modified bessel function of the first kind, zeroth order.
- I_1 modified bessel function of the first kind, first order.
- J_0 bessel function of the first kind, zeroth order.
- J_1 bessel function of the first kind, first order.
- k hydraulic conductivity, L/T.
- k_D dimensionless hydraulic conductivity.
- K_0 modified bessel function of the second kind, zeroth order.
- K_1 modified bessel function of the second kind, first order.
- L length, L.
- n number of fractures intersecting well.
- p Laplace variable.
- Q well flow rate, L^3/T.
- r radial distance, L.
- r_c ratio of well bore radius to inner region radius.
- r_D dimensionless radial distance.
- r_e distance to outer boundary, L.
- r_f inner region radius, L.
- r_w well bore radius, L.
- r_w' apparent well bore radius, L.
- R distance to discontinuity, L.
- S storativity.
- S_s specific storage, $1/L$.
- S_{sD} dimensionless storage.
- t time, T.
- t_s dimensionless time.
- T transmissivity, L^2/T.
- x_D dimensionless distance, L.
- Y_0 bessel function of the second kind, zeroth order.
- Y_1 bessel function of the second kind, first order.
- α diffusivity, L^2/T.
- α_c dimensionless diffusivity.
- β dimensionless tranmissivity.
- γ storage ratio of layer 2 to layer 1.
- ω storage ratio of formation to well.
- ρ fluid density, M/L^3.

Subscripts

- D dimensionless.
- i initial.
- f based on fracture.
- s dimensionless.
- w well bore.
- 0 initially applied value.
- 1 region 1.
- 2 region 2.

Acknowledgments. This work was supported by the U.S. Geological Survey, Denver, Nuclear Hydrology Program directed by Bill Wilson through the U.S. Department of Energy (DOE) under contract DE-AC03-76-SF00098 via the DOE Nevada Office.

REFERENCES

Barker, J. A., and J. H. Black, Slug tests in fissured aquifers, *Water Resour. Res.*, *19*(6), 1558–1564, 1983.

Bourdet, D., T. M. Whittle, A. A. Douglas, and Y. M. Pirard, A new set of type curves simplifies well test analysis, *World Oil*, *196*, 95–106, 1983.

Carslaw, H. S., and J. C. Jaeger, *Conduction of Heat in Solids*, Clarendon Press, Oxford, 1946.

Cooper, H. H., Jr., J. D. Bredehoeft, and I. S. Papadopulos, Response of a finite diameter well to an instantaneous charge of water, *Water Resour. Res.*, *3*, 263–269, 1967.

Faust, C. R., and J. W. Mercer, Evaluation of slug tests in wells containing a finite radius skin, *Water Resour. Res.*, *20*(4), 504–506, 1984.

Ferris, J. G., and D. B. Knowles, The slug test for estimating transmissivity, *U.S. Ground Water Note*, *26*, 1954.

Ferris, J. G., D. B. Knowles, R. H. Brown, and R. W. Stallman, Theory of aquifer tests, *U.S. Geol Surv. Water Supply Pap.*, *1536-E*, 1962.

Karasaki, K., Well test analysis in fractured media, Ph.D. dissertation, 239 pp., Univ. of Calif., Berkeley, 1986.

Karasaki, K., J. C. S. Long, and P. A. Witherspoon, A new analytical model for fracture-dominated reservoirs, *Soc. Pet. Eng. J.*, in press, 1988.

Lefkovits, H. C., P. Hazebroek, E. E. Allen, and C. S. Matthews, A study of the behavior of bounded reservoirs composed of stratified layers, *Soc. Pet. Eng. J.*, *1*, 43–58, 1961.

Moench, A. F., and P. A. Hsieh, Analysis of slug test data in a well with finite thickness skin, paper presented at the I.A.H. 17th International Congress on Hydrology of rocks of low permeability, Int. Assoc. of Hydrogeol., Tucson, Ariz., Jan. 7–12, 1985.

Ogbe, D. O., and W. E. Brigham, A model for interference testing with wellbore storage and skin effects at both wells, paper presented at the 59th Annual Technical Conference and Exhibition, Soc. Petrol. Eng., Houston, Tex., Sept. 16–19, 1984.

Ramey, H. J., Jr., and R. G. Agarwal, Annulus unloading rates as influenced by wellbore storage and skin effect, *Soc. Pet. Eng. J.*, *253*, 453–462, 1972.

Ramey, H. J., Jr., R. G. Agarwal, and I. Martin, Analysis of "slug test" or DST flow period data, *J. Can. Pet. Technol.*, *14*, 37–47, 1975.

Russell, D. G., and M. Prats, Performance of layered reservoirs with crossflow single-compressible-fluid case, *Soc. Pet. Eng. J.*, *2*, 53–67, 1962.

Sageev, A., Slug test analysis, *Water Resour. Res.*, *22*(8), 1323–1333, 1986.

Stehfest, H., Algorithm 368 numerical inversion of Laplace transforms, D-5, *Commun. ACM*, *13*(1), 47–49, 1970.

Tongpenyai, Y., and R. Raghavan, The effect of wellbore storage and skin on interference test data, *J. Pet. Technol.*, *33*, 151–160, 1981.

Wang, J. S. Y., T. N. Narasimhan, C. F. Tsang, and P. A. Witherspoon, Transient flow in tight fractures, paper presented at Proceedings, Invitational Well Testing Symposium, Lawrence Berkeley Lab., Berkeley, Ca., Oct. 19–21, 1977.

K. Karasaki, J. C. S. Long, and P. A. Witherspoon, Lawrence Berkeley Laboratory, Earth Sciences Division, University of California, 1 Cyclotron Road, Berkeley, CA 94720.

(Received November 26, 1986;
revised September 21, 1987;
accepted September 22, 1987.)